# Transport of a persistent spin helix drifting transverse to the spin texture

F. Passmann,[1] A. D. Bristow,[1,2,*] J. N. Moore,[3] G. Yusa,[3,4] T. Mano,[5] T. Noda,[5] M. Betz,[1,†] and S. Anghel[1]

[1]*Experimentelle Physik 2, Technische Universität Dortmund, Otto-Hahn-Straße 4a, D-44227 Dortmund, Germany*

[2]*Department of Physics and Astronomy, West Virginia University, Morgantown, West Virginia 26506-6315, USA*

[3]*Department of Physics, Tohoku University, Sendai 980-8578, Japan*

[4]*Center for Spintronics Research Network, Tohoku University, Sendai 980-8578, Japan*

[5]*National Institute for Materials Science, Tsukuba, Ibaraki 305-0047, Japan*

(Received 25 January 2019; published 4 March 2019)

Time-resolved magneto-optic Kerr microscopy measures the effect of in-plane electric fields on the dynamics of a photoexcited spin distribution in a modulation-doped GaAs quantum well. The structure features nearly equal Dresselhaus and Rashba coefficients, such that there is negligible impact of spin-orbit coupling for electrons moving along the $[1\bar{1}0]$ or $[\bar{1}10]$ directions. Meanwhile, spin texture emerges for electrons moving in the [110] or $[\bar{1}\bar{1}0]$ directions. The overall spin pattern resembles a persistent spin helix. An in-plane electric field, applied transverse to the spin texture (along the $[1\bar{1}0]$ or $[\bar{1}10]$ directions), introduces a drift of the spin packet and additional Larmor precessions, i.e., a marked decrease of the spatial periodicity of the spin pattern. The in-plane electric field also increases the temporal frequency of the evolving spin distribution, which is directly linked to the cubic Dresselhaus spin-orbit coupling term. Moreover, the in-plane field increases the diffusion coefficient by more than an order of magnitude. We attribute this effect to carrier heating and the separation of the photogenerated electron-hole dipole.

DOI: 10.1103/PhysRevB.99.125404

## I. INTRODUCTION

The allure of controlled spin transport in semiconductors is a challenge that requires manipulating the spin-orbit (SO) coupling within the transport medium [1]. III-V zinc-blende semiconductors inherently have SO coupling due to the bulk inversion asymmetry [2] and can comprise heterostructures that produce further inversion asymmetry as a result of built-in electric fields [3,4]. These Dresselhaus and Rashba SO coupling contributions can be tuned by material composition and structural design, profoundly affecting spin transport by producing a momentum-dependent effective magnetic field $\boldsymbol{B}_{\mathrm{SO}}(\boldsymbol{k})$. An example of this is the persistent spin helix (PSH) in a two-dimensional electron gas (2DEG) [5,6], where Dresselhaus ($\beta$) and Rashba ($\alpha$) coefficients are made to be equal ($\beta/\alpha = 1$) [7,8], giving an SU(2) symmetry of $\boldsymbol{B}_{\mathrm{SO}}(\boldsymbol{k})$ so that no Larmor precession is observed for diffusive transport along the $[1\bar{1}0]$ and $[\bar{1}10]$ directions. The SU(2) symmetry suppresses D'yakanov-Perel scattering and increases the spin lifetime for the PSH mode, which is then defined by a single long-lived mode with a spin precession length $\lambda_0$ [9].

PSH manipulation in zinc-blende semiconductor 2DEGs has been demonstrated in various ways. Applied in-plane magnetic fields have been used to determine the $\alpha$ and $\beta$ parameters [7,10–12]. Out-of-plane electrical fields have been used to modify $\beta/\alpha$ and the 2DEG carrier mobility [7,8,13–15]. Dual modulation-doping geometries demonstrate stretchable PSH modes by tuning $\alpha$ and $\beta$ together [16]. Optical doping has shown an excitation-density dependence of $\alpha$, $\beta$, and the spin diffusion coefficient $D_s$ [17]. Application of in-plane electric fields has been used to introduce a spin drift velocity, $v_{\mathrm{dr}}$, revealing a modification of the spatial extent of the spin distribution with time, $\lambda_{\mathrm{so}}(t)$ [1,14,18–20], and a temporal oscillation of the spin polarization due to the cubic Dresselhaus contribution $\beta_3$. The latter is an extension from the linear contribution $\beta_1$, such that the Dresselhaus SO coefficient becomes $\beta = \beta_1 - \beta_3$.

To date, most in-plane electric-field studies have been performed in GaAs-based 2DEGs, focused on moderate drift velocities along the [110] (and $[\bar{1}\bar{1}0]$) direction $||y$ for convenience, where there is significant Larmor precession due to the symmetry of $B_{\mathrm{so}}$. There are limited data on the spin transport in the $[1\bar{1}0]$ (or $[\bar{1}10]$) direction $||x$ [19], where effects of $B_{\mathrm{so}}$ are negligible without increasing the electron momentum by an applied in-plane electric field and the observed Larmor precession has an extremely long $\lambda_{\mathrm{so}}(t)$ at all times. Hence, determining the interplay of drift and diffusion for applied electric fields in these directions is appealing because of the *clean* (zero-field) control experiment. In this paper, we explore spin transport along the $x$ direction of a modulation-doped GaAs 2DEG that has SO coupling close to the PSH regime. Experiments are performed by time-resolved Kerr-rotation microscopy (TR-KRM) with an adjustable in-plane electric field to control the drift velocity, $v_{\mathrm{dr}}$, of the excited spin polarization. Varying the drift velocity reveals changes in the spatiotemporal evolution of the spin-profile that are consistent with increased diffusion and decreased spin precession length [14]. The experiments directly access the previously unobtainable spin precession length along the $x$ direction, $\lambda_{0,x}$, and the cubic Dresselhaus SO coefficient, $\beta_3$.

*alan.bristow@mail.wvu.edu

†markus.betz@tu-dortmund.de

 

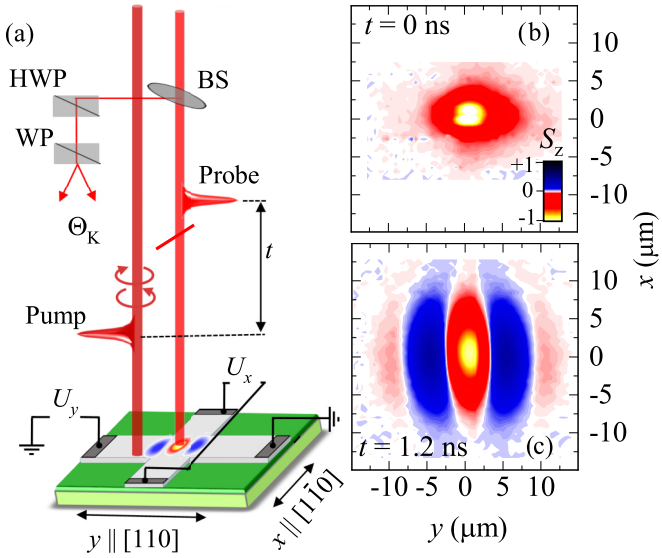


FIG. 1. (a) Experimental setup for time-resolved Kerr-rotation microscopy of the 2DEG with Hall-bar geometry and in-plane electric fields applied by voltages ($U_x$, $U_y$), where $x \parallel [110]$ and $y \parallel [1\bar{1}0]$. ($t$ = delay time, BS = beam splitter, HWP = half − wave plate, WP = Wollaston prism, $\theta_K$ = Kerr-rotation signal.) Spin-polarization micrographs $S_z(x, y, t)$ where (b) $t = 0$ ns and (c) 1.2 ns. The same color bar applies for all the subsequent figures.

## II. EXPERIMENT

Figure 1(a) shows the geometry of the 2DEG with electrical contacts and the TR-KRM. The sample is grown by molecular beam epitaxy on a highly $n$-doped [001]-cut GaAs substrate. The epistructure consists of a 15-nm-thick GaAs quantum well sandwiched between $Al_{0.33}Ga_{0.67}As$ barriers and a Si $\delta$-doping layer, providing a resident carrier concentration. The wafer is patterned in a 15-$\mu$m-wide Hall-bar geometry with a back gate and AuGeNi Ohmic in-plane contacts. The dimensions between the in-plane contacts are $d_x = 1.107 \pm 0.001$ mm and $d_y = 1.145 \pm 0.001$ mm. Measurements presented herein are performed with a back-gate voltage $U_{BG} \approx -1$ V and a lattice temperature of 3.5 K to maximize the spin lifetime. From magnetotransport, photoluminescence, and transient reflectivity measurements it is estimated that the carrier concentration is $n_e \approx 9 \times 10^{10}$ cm$^{-2}$, mobility is $\mu \approx 2.5 \times 10^5$ cm$^2$/(V s), and photocarrier lifetime is $\tau > 670$ ps. The Fermi energy is $E_F = \hbar^2 \pi n_e / m^* \approx 3$ meV above the conduction band minimum, where $m^* = 0.064 m_e$ is the electron effective mass [21], $m_e$ is the fundamental electron mass, and $\hbar$ is the reduced Planck constant.

TR-KRM is performed with ∼35-fs laser pulses derived from a 60-MHz mode-locked Ti:sapphire oscillator. Pulses are split into a pump and probe path that are independently tuned by grating-based pulse shapers [15], resulting in pulses with a bandwidths of ∼0.5 nm and temporal resolution of ∼1 ps. Pump pulses impinge the sample at normal incidence with modulated left $\sigma^+$ and right $\sigma^-$ circular polarization by means of an electro-optic modulator and focused through a 50× microscope objective to a full width at half maximum (FWHM) diameter of $w_0 = 3 \pm 0.1$ $\mu$m. Linearly polarized probe pulses are reflected from the sample through the same objective with a FWHM diameter of $1 \pm 0.1$ $\mu$m. The reflection is filtered by a monochromator and polarization resolved using a half-wave plate and Wollaston prism. Kerr rotation is measured with balanced photodiodes feeding a lock-in amplifier referenced to the electro-optic modulation frequency. The delay time $t$ between the pump and probe pulses is adjusted by a mechanical delay stage with $t_{max} = 1.7$ ns. The spatial overlap of the pump with the fixed and centered (at the crossing of the Hall-bar structure) probe is adjusted through the axis of the input lens to the beam-expanding telescope in the pump path [22,23]. Measurements are performed with pump and probe pulse energies and peak irradiances set to $E_p \approx 1.57$ eV, $E_{pr} \approx 1.53$ eV, $I_p \approx 3.53$ MW/cm$^2$, and $I_{pr} \approx 2.36$ MW/cm$^2$. The pump and probe photon energies are chosen based on the spectral response of the 2DEG at maximum spatial and temporal overlap; see Ref. [14].

## III. RESULTS

Kerr-rotation micrographs in the $xy$ plane are shown in Fig. 1(b) at $t = 0$ ps and Fig. 1(c) 1.2 ns for $E_x = 0$ V/cm. Comparison illustrates the diffusive expansion of the spin polarization $S_z(x, y, t)$ due to finite spot-size effect [24], wherein the photoexcitation of electrons adds to the 2DEG and transfers spin angular momentum from photons to electrons, resulting in a net spin-polarized ensemble. With increasing time, diffusion leads to spin polarization with a larger spatial extent and Larmor precession along the $y$ axis due to the PSH regime. Using these data in conjunction with data for applied in-plane magnetic field (not shown), it is estimated that $D_s = 50 \pm 3$ cm$^2$/s in both $x$ and $y$ directions, $\alpha = 0.9 \pm 0.1$ meV Å and $\beta = 2.1 \pm 0.1$ meV Å, based on the $k$-dependent effective magnetic field being proportional to $\alpha + \beta$ and $\alpha - \beta$ for spins diffusing in the $y$ and $x$ directions respectively. Consequently, it is expected that $\lambda_{0,x} = \pi\hbar^2/[m^*(\alpha - \beta)] = 32 \pm 0.3$ $\mu$m and $\lambda_{0,y} = \pi\hbar^2/[m^*(\alpha + \beta)] = 11 \pm 0.3$ $\mu$m [7].

TR-KRM measurements are performed over a bipolar range of in-plane voltages up to $|E_x| = 12$ V/cm (corresponding to a current of $I = 218$ $\mu$A). Figures 2(a)–2(c) show representative $S_z(x, 0, t)$ data for $E_x = 0$, −3.4, and −10.2 V/cm respectively, for which the corresponding drift velocities are $v_{dr} \approx 0$, 7.8, and 30.0 km/s, extracted from the evolution of the moving spin packet. Consequently, we extract a mobility of $\mu = -v_{dr}/E_x \approx (2.8 \pm 0.5) \times 10^5$ cm$^2$/(V s), comparable to the one from magnetotransport measurements. For zero drift velocity, the Kerr-rotation signal is stationary (centered at $x = 0$ $\mu$m) and decays in time, resulting in the vertical transient. For the two cases of increased $v_{dr}$, the spin distribution moves along $x$ with different speeds proportional to $E_x$. The motion introduces Larmor precession along $x$, with a slow oscillation in $t$ as indicated by tilted, dashed lines in the plot. In addition, the increasing $v_{dr}$ causes a spatial broadening of the entire distribution and a reduction in the signal lifetime.

Slices in the $x$ direction are extracted at $t \approx 0.6$ ns for comparison; see Fig. 2(d). For $E_x = 0$ V/cm, the slice reveals a Gaussian feature of width $w(t) = \sqrt{w_0^2 + 16 \ln(2) D_s t}$ (with initial width $w_0$ based on the excitation spot) that has not undergone visible Larmor precession, despite moderate diffusion. The other slices confirm the broadening and show evidence of the momentary spin precession length $\lambda_{so}(t) =$

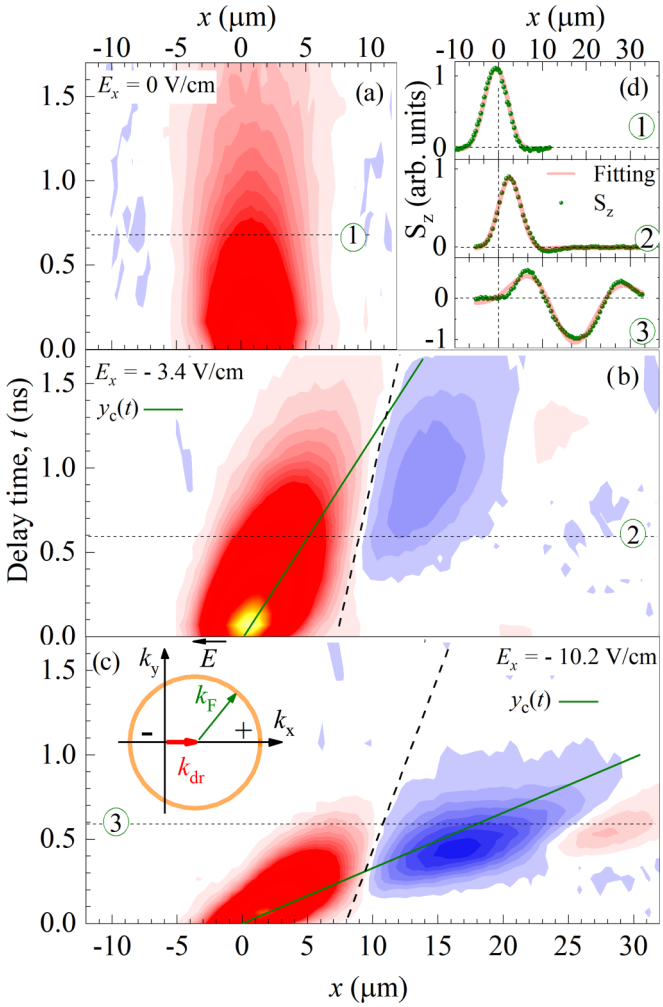


FIG. 2. Spin polarization $S_z(x, 0, t)$ for electric fields, corresponding to in-plane voltages (a) $E_x = 0$ V/cm, (b) $-3.4$ V/cm, and (c) $-10.2$ V/cm. Construction lines highlight the motion of center of the spin polarization due to drift velocity $v_{dr}t$ (solid) and temporal precession (dashed) and spatial slices (dotted). (d) Experimental slices $S_z(x = 0, t \approx 0.6\,\text{ns})$ for the same three electric fields are shown in (a)–(c) with their respective fits. The inset in (c) shows drift of the in-plane Fermi circle along the $x$ axis.

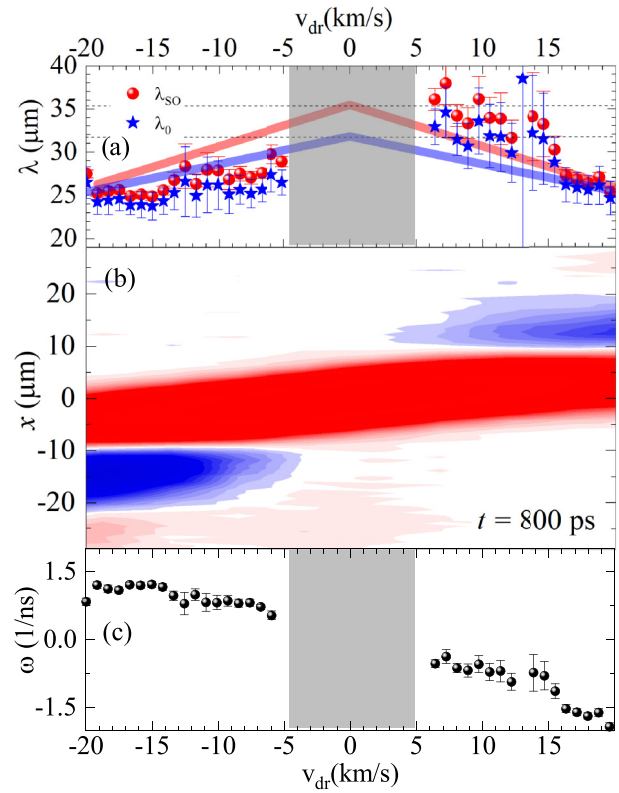


FIG. 3. (b) Spin polarization $S_z(x, 0, 0.8\,\text{ns})$ for a range of electric fields corresponding to drift velocities up to $v_{dr} = \pm 20$ km/s. (a) Extracted spin precession length $\lambda_{SO}(v_{dr})$ and estimated $\lambda_0(v_{dr})$ together with absolute value fitting functions, allowing to extract $\lambda_{SO}(v_{dr} = 0)$ and $\lambda_0(v_{dr} = 0)$. (c) Angular frequency $\omega(v_{dr})$.

$\lambda_0 w(t)^2/[w(t)^2 - w_0^2]$. The slices (and the entire spatiotemporal data) are typically characterized in terms of the expression $S_z(x, 0, t) = A \exp[-4\ln(2)x^2/w^2]\cos(qx + \omega t)$, where $A$ is the spin polarization amplitude, $q = 2\pi/\lambda_{so}$ is the wave vector associated with spin texture, and $\omega = -(2m^*/\hbar^2)v_{dr}\beta_3$ is the angular frequency of oscillations in the time domain [19]. Examples of the fit quality are also shown in the figure.

The quantities $q$ and $\omega$ are derived from the effective magnetic field $\boldsymbol{B}_{SO}(\boldsymbol{k}) = 2[(-\alpha + \beta_1)(k_{dr,x} + k_{diff,x}) - \beta_3(2k_{dr,x} + k_{diff,x})]/g\mu_B$, where $g$ is the effective $g$-factor, $\mu_B$ is the Bohr magneton, and $k_{dr,x}$ and $k_{diff,x}$ are the $x$-direction projections of the drift and diffusion wave vectors $\boldsymbol{k}_{dr}$ and $\boldsymbol{k}_{diff}$ throughout the plane of the 2DEG; see the illustration inset in Fig. 2(c). The above relation, derived by Altmann *et al.* [19], illustrates that the effect of drift ($\boldsymbol{k}_{dr,x}$) on the precession angle is larger than that from diffusion ($\boldsymbol{k}_{diff,x}$). Hence, as the spin packet evolves, the spin polarization at any point in $x$ is a superposition of spins that have undergone drift only with spins that have undergone both drift and diffusion. The different transport contributions lead to spin precession in time at any position in $x$.

Figure 3(b) shows the $S_z(x, 0, t = 0.8\,\text{ns})$ for $5\,\text{V/cm} \leqslant E_x \leqslant -5\,\text{V/cm}$, corresponding to $-20\,\text{km/s} \leqslant v_{dr} \leqslant 20\,\text{km/s}$. Hence, for fixed optical excitation conditions, this gives access to the effect of $k_{dr,x}$ directly. The time is chosen to allow for fitting clear oscillations in $x$ throughout the range of $v_{dr}$. First, varying the in-plane voltage shifts the spin distribution linearly about $x = 0\,\mu$m, such that at $x \approx \pm 15\,\mu$m ($v_{dr} \approx \pm 5$ km/s) the spins signal has rotated by $\pi$ due to the motional Larmor precession. Second, the width of the signal distribution increases with increasing $|v_{dr}|$, making it wider at the extremes than in the center.

## IV. DISCUSSION

Since the delay time in Fig. 3(b) is fixed, $\lambda_{so}(v_{dr})$ corresponds to the periodicity of the cosine fitting term in the $x$-direction slices and is plotted in Fig. 3(a). The central region is not shown, due to low oscillation frequency. It is seen that $\lambda_{so}$ decreases somewhat symmetrically with increasing $v_{dr}$, which is the same trend seen along the $y$ direction [14]. The variation of $\lambda_{so}$ with drift velocity results from a modification of SO coupling parameters, where a contribution to $\alpha$ is unlikely due to geometry, and thus a modification of $\beta$ is

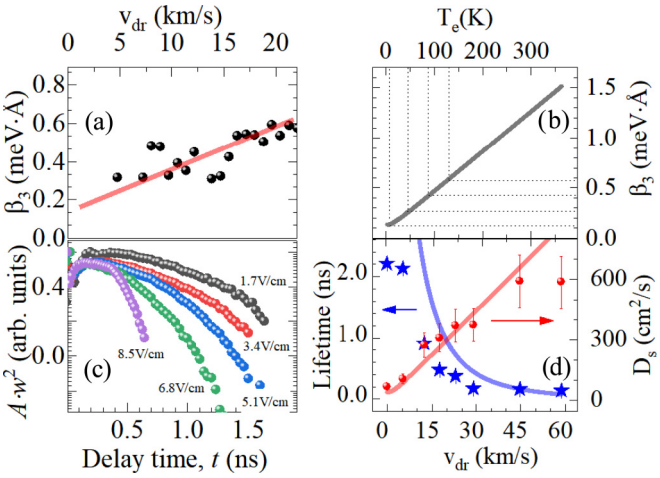


FIG. 4. (a) Experimental cubic Dresselhaus SO coupling term $\beta_3(v_{dr})$ and the best fit. (b) Calculated $\beta_3(T_e)$ showing the estimated electron temperature $T_e$ achieved in the drift velocity range of Fig. 3 and extrapolation to higher values of $\beta_3$. (c) Spin volume $\{A(t)w^2(t)\}$ transients for several in-plane electric-field values. (d) Extracted spin lifetimes $\tau_s$ determined from the spin volume and spin diffusion coefficient $D_s$ extracted directly from $S_z(x, 0, t)$ as a function of $v_{dr}$. Modeled $D_s$ and $\tau_s$ are shown as solid lines, revealing a $T_e$ range comparable to that estimated in (b).

probable. From the figure, as $v_{dr} = 0\,\mathrm{km/s}$, $\lambda_{so}(t = 0.8\,\mathrm{ns}) \approx 36 \pm 3\,\mu\mathrm{m} \rightarrow \lambda_0 \approx 30 \pm 3\,\mu\mathrm{m}$, using $D_s(0\,\mathrm{V}) = 50\,\mathrm{cm}^2/\mathrm{s}$, which compares favorably to the estimates of $\lambda_0$ obtained from magnetic-field measurements. This $E_x$-measurement value is slightly smaller with larger error, because the spin polarization is still decaying towards $\lambda_0$ and the estimate is extracted at a single delay time. Nonetheless, applied in-plane electric-field measurements are used to directly estimate the PSH spin precession length at zero electric field.

Figure 3(c) shows the extracted $\omega(v_{dr})$ to decrease monotonically throughout the range of $v_{dr}$. This corresponds to a phase shift of the cosine fitting term from the center position of the spin distribution, which has only previously been seen along the $y$ axis. A sloped $\omega(v_{dr})$ is consistent with the discussion regarding its relation to the cubic Dresselhaus SO coupling parameter. It is also possible that $\beta_3$ also depends on the drift velocity because it is dependent on the Fermi energy of the 2DEG, $\beta_3 = \gamma m^* E_F/2\hbar^2 = 0.14\,\mathrm{meV\,\AA}$, where the Dresselhaus parameter for GaAs is $\gamma = 11\,\mathrm{eV\,\AA}^3$. Increasing $v_{dr}$ adds kinetic energy to the Fermi velocity of the 2DEG electrons, equivalent to heating the electron gas. This leads to a transition from degenerate (Fermi-Dirac) to nondegenerate statistics (Boltzmann) [18]. The resulting average electron energy is then given as $\varepsilon = E_F/[1 - \exp(-E_F/k_B T_e)]$, where $k_B$ is the Boltzmann constant and $T_e$ is the electron temperature. At $T_e \rightarrow 0\,\mathrm{K}$, $\beta_3$ is the value determined for the unheated Fermi wave vector $k_F = \sqrt{2m^* E_F}/\hbar$. At all other temperatures, Fermi smearing occurs and the cubic Dresselhaus SO coupling becomes $\beta_3(T_e) = \gamma m^* \langle\varepsilon\rangle/2\hbar^2$. At high enough $T_e$ this contribution is linear, i.e., $\beta_3 = \gamma m^*/2\hbar^2(E_F/2 + k_B T_e)$. Figure 4(a) shows the extracted $\beta_3(v_{dr})$, along with the zero-field value and a linear fit. For comparison, Fig. 4(b) shows theoretical $\beta_3(T_e)$, using known sample parameters. It is conceivable that for in-plane voltages of $|E_x| = 12\,\mathrm{V/cm}$, the temperature of the 2DEG could reach ~300 K, because the high mobility indicates low electron-phonon coupling. The momentum scattering time is estimated to be $\tau_k \approx 12.7\,\mathrm{ps}$, as compared to a substantially larger energy relaxation time $\tau_E$ [25]. Consequently, the energy deposited into an electron during its time of flight in the 10 V/cm field is $E = (eE_x\tau_E)^2/2m^* \approx 14.8\,\mathrm{meV}$, which is equivalent to an electron temperature of ~170 K. This temperature is below the longitudinal optical (LO) phonon energy at 36 meV, or ~400 K.

From the spatiotemporal data, it is seen that the lifetime of the spin signal is also reduced with increasing drift velocity. Figure 4(c) shows the extracted spin volume ($Aw^2$) plotted as a function of delay time, determined from fitting the spatiotemporal data for several in-plane electric fields. The transient spin volume has a nonexponential decay, due to a drastic increase in decay slope at large $t$. The slope change also occurs earlier in delay time with increasing $v_{dr}$. In principle, the spin volume captures the entire moving spin polarization throughout $t$, avoiding optical vignetting by scanning the microscope objective. Analysis of the decay of the spin volume gives representative spin lifetimes as a function of $v_{dr}$; see Fig. 4(d). The spin lifetime is given as $\tau_s^{-1} \approx 2D_s(m^{*2}/\hbar^4)[3\beta_3^2 + (\alpha - \beta_1 + \beta_3)^2]$ [7], suggesting that its $v_{dr}$-dependent decrease is influenced by both $\beta_3$ and $D_s$. As observed in the spatiotemporal data, $D_s$ does appear to vary with $v_{dr}$. $D_s$ is extracted independently by fitting the Gaussian width of $S_z(x, 0, t)$ over a limited time range ($0.3\,\mathrm{ns} < t < 0.7\,\mathrm{ns}$), as plotted in Fig. 4(d). The $t$ limit ensures at least half a spatial oscillation and avoids the strongly decayed signal for larger $v_{dr}$. The increasing $D_s$ further verifies the broadening of the spatial extent of the spin distribution with increasing $v_{dr}$ and is consistent with the resulting model of increased $T_e$. Hence, $D_s = \tau_k E_F/m^*$ must also be determined by replacing the Fermi energy with $\langle\varepsilon\rangle$. The model of $D_s(T_e)$ is well matched to the data in Fig. 4(d) throughout the range of $T_e$ estimated from $\beta_3$ in Figs. 4(a) and 4(b). Finally, with both $\beta_3$ and $D_s$ dependences on $v_{dr}$ determined, $\tau_s$ can also be modeled, resulting in an asymptotic behavior that represents the extracted data well.

Up to some moderate value, $v_{dr}$ increases $D_s$, decreases $\tau_s$, and increases $|\beta_3|$. At drift velocities above 45 km/s, $D_s$ matches quite well but appears to roll over. One possible mechanism for this is coupling to LO phonons, which has been observed to occur below the LO phonon resonance at electron temperatures as low as ~100 K [26–28]. In this case, temperatures $T_e(v_{dr})$ would saturate or be sublinear. Additionally, increasing temperature increases the electron heat capacity [29], suggesting that while the drift velocity is linearly increased with in-plane voltage the resulting $T_e$ is sublinear.

After examining the phonons and thermodynamics, $T_e$ alone may be insufficient to explain the observed increase in $D_s$. In fact, in one-dimensional $S_z(x)$ at fixed $y$ and $t$, $D_s$ may also include changes in mobility. Hence, an alternative source of the increasing $D_s$ with $v_{dr}$ may be an increase in $\tau_s$ through unbound charge separation. As photogenerated electrons and holes separate under the influence of the applied field, the mean free path (or time between scattering events) can increase for the spin-polarized charge carriers. A strongly increasing $D_s$ is likely to change the slope of the spin volume

transient at some time during the decay. Moreover, it would be expected to occur earlier in time as the drift velocity increases and there is a characteristic time at which charge separation has occurred, $t_{cs}$. Both the slope change and its arrival earlier in time are exhibited in $Aw^2$; see Fig 4(c). Indeed, using $t_{cs} \approx w(t_{cs})/v_{dr}$ to represent the delay time where the transient would steepen, due to charge separation and increased diffusion, reveals self-consistent values based on inputting the estimated values of $v_{dr}$, $D_s$, and $t_{cs}$. This suggests that increasing $v_d$ is expected to hasten the onset of the steeper slope due to charge separation. Moreover, this mechanism explains the increase of the $D_s$ at higher fields where carrier heating may be less effective.

Finally, using the calculated $D_s$ values to estimate $\lambda_0$ in Fig. 3(a) shows that the slope is less steep than $\lambda_{SO}$. This is expected because $\lambda_0$ is equivalent to choosing a large delay time, where the spin distribution has relaxed into the PSH mode. Comparison to Ref. [18] shows a trend of $k_{SO}$ that decreases with increasing $v_{dr}$. In this case, continuous-wave measurements sample $\lambda_0$ and are minimally effected by diffusion. In time-resolved measurements, $\lambda_{SO}$ only approaches $\lambda_0$ with increasing time. For large enough time delay and differing sample parameters, $\lambda_0(v_{dr})$ may result in different slopes [19].

## V. CONCLUSION

In conclusion, the systematic variation of an in-plane electric field in a 2DEG is governed by the SO coupling, even in systems close to the persistent spin helix regime, where one direction should have a negligible effective magnetic field. In zero field, spins moving in the $x$ direction ($[1\bar{1}0]$ or $[\bar{1}10]$) do not undergo spin precession, which offers a good control for the effects introduced to spins moving with a drift velocity. The observations show that the cubic Dresselhaus parameters govern any drift-dependent spin precession; the spin packet undergoes additional diffusion and a reduction in the spin lifetime. The latter properties are consistent with an increased electron temperature and charge separation, due to the applied electric field. Moreover, the $x$-direction TR-KRM measurements allow for determination of $\alpha - \beta$ from the spin precession length $\lambda_{0,x}$ without the application of an external magnetic field. Combining this result with $\alpha + \beta$, readily extracted from $\lambda_{0,y}$, provides a method for independent extraction of $\alpha$ and $\beta$ without the use of a magnet.

## ACKNOWLEDGMENTS

The authors wish to thank Alexander Poshakinskiy and Sergey Tarasenko from the Ioffe Institute for useful discussions. Funding was provided by the Deutsche Forschungsgemeinschaft International Collaborative Research Centre TRR 160 (Project No. 249492093, subproject B3). This work was supported by a Grant-in-Aid for Scientific Research (Grant No. 17H01037) from the Ministry of Education, Culture, Sports, Science, and Technology (MEXT), Japan, and the Asahi Glass Foundation.

[1] Y. Kunihashi, H. Sanada, H. Gotoh, K. Onomitsu, M. Kohda, J. Nitta, and T. Sogawa, Nat. Commun. **7**, 10722 (2016).
[2] G. Dresselhaus, Phys. Rev. **100**, 580 (1955).
[3] E. I. Rashba and A. L. Efros, Phys. Rev. Lett. **91**, 126405 (2003).
[4] E. I. Rashba, Fiz. Tverd. Tela (Leningrad) **2**, 1224 (1960).
[5] B. A. Bernevig, J. Orenstein, and S. C. Zhang, Phys. Rev. Lett. **97**, 236601 (2006).
[6] S. D. Ganichev and L. E. Golub, Phys. Status Solidi B **251**, 1801 (2014).
[7] M. P. Walser, C. Reichl, W. Wegscheider, and G. Salis, Nat. Phys. **8**, 757 (2012).
[8] M. Studer, G. Salis, K. Ensslin, D. C. Driscoll, and A. C. Gossard, Phys. Rev. Lett. **103**, 027201 (2009).
[9] V. N. Gridnev, J. Exp. Theor. Phys. Lett. **76**, 502 (2002).
[10] A. Sasaki, S. Nonaka, Y. Kunihashi, M. Kohda, T. Bauernfeind, T. Dollinger, K. Richter, and J. Nitta, Nat. Nanotechnol. **9**, 703 (2014).
[11] M. Kohda, V. Lechner, Y. Kunihashi, T. Dollinger, P. Olbrich, C. Schönhuber, I. Caspers, V. V. Bel'kov, L. E. Golub, D. Weiss, K. Richter, J. Nitta, and S. D. Ganichev, Phys. Rev. B **86**, 081306(R) (2012).
[12] T. Yusuke, K. Yoji, S. Haruki, G. Hideki, O. Koji, K. Makoto, N. Junsaku, and S. Tetsuomi, Appl. Phys. Express **12**, 013001 (2019).
[13] P. Altmann, M. P. Walser, C. Reichl, W. Wegscheider, and G. Salis, Phys. Rev. B **90**, 201306 (2014).
[14] S. Anghel, F. Passmann, A. Singh, C. Ruppert, A. V. Poshakinskiy, S. A. Tarasenko, J. N. Moore, G. Yusa, T. Mano, T. Noda, X. Li, A. D. Bristow, and M. Betz, Phys. Rev. B **97**, 125410 (2018).
[15] S. Anghel, A. Singh, F. Passmann, H. Iwata, J. N. Moore, G. Yusa, X. Li, and M. Betz, Phys. Rev. B **94**, 035303 (2016).
[16] F. Dettwiler, J. Y. Fu, S. Mack, P. J. Weigele, J. C. Egues, D. D. Awschalom, and D. M. Zumbuhl, Phys. Rev. X **7**, 031010 (2017).
[17] F. Passmann, S. Anghel, T. Tischler, A. V. Poshakinskiy, S. A. Tarasenko, G. Karczewski, T. Wojtowicz, A. D. Bristow, and M. Betz, Phys. Rev. B **97**, 201413(R) (2018).
[18] Y. Kunihashi, H. Sanada, Y. Tanaka, H. Gotoh, K. Onomitsu, K. Nakagawara, M. Kohda, J. Nitta, and T. Sogawa, Phys. Rev. Lett. **119**, 187703 (2017).
[19] P. Altmann, F. G. G. Hernandez, G. J. Ferreira, M. Kohda, C. Reichl, W. Wegscheider, and G. Salis, Phys. Rev. Lett. **116**, 196802 (2016).
[20] M. Schwemmer, A. Hanninger, M. Weingartner, M. Oltscher, M. Ciorga, D. Weiss, D. Schuh, D. Bougeard, T. Korn, and C. Schuller, Appl. Phys. Lett. **109**, 172106 (2016).
[21] A. Raymond, J. L. Robert, and C. Bernard, J Phys. C: Solid State Phys. **12**, 2289 (1979).
[22] T. Henn, T. Kießling, L. W. Molenkamp, D. Reuter, A. D. Wieck, K. Biermann, P. V. Santos, and W. Ossau, Phys. Status Solidi B **251**, 1839 (2014).

[23] T. Henn, T. Kiessling, W. Ossau, L. W. Molenkamp, K. Biermann, and P. V. Santos, Rev. Sci. Instrum. **84**, 123903 (2013).

[24] G. Salis, M. P. Walser, P. Altmann, C. Reichl, and W. Wegscheider, Phys. Rev. B **89**, 045304 (2014).

[25] T. C. Damen, L. Viña, J. E. Cunningham, J. Shah, and L. J. Sham, Phys. Rev. Lett. **67**, 3432 (1991).

[26] J. Shah, A. Pinczuk, H. L. Störmer, A. C. Gossard, and W. Wiegmann, Appl. Phys. Lett. **44**, 322 (1984).

[27] J. Shah, A. Pinczuk, H. L. Störmer, A. C. Gossard, and W. Wiegmann, Appl. Phys. Lett. **42**, 55 (1983).

[28] C. H. Yang, J. M. Carlson-Swindle, S. A. Lyon, and J. M. Worlock, Phys. Rev. Lett. **55**, 2359 (1985).

[29] C. Kittel, *Introduction to Solid State Physics*, 8th ed. (John Wiley and Sons, Inc., New York, 2005).